Étude des performances du cycle frigorifique régénératif de Brayton utilisant un nouveau matériau composite Mn-Fe-P-Si avec hystérésis thermique comme milieu de travail

Li, Yan; Huang, Bowei; Lin, Guoxing; Chen, Jincan; Brück, Ekkes

DOI
10.1016/j.ijrefrig.2021.12.018

Publication date
2022

Document Version
Final published version

Published in
International Journal of Refrigeration

International Journal of Refrigeration 135 (2022) 20–28

Contents lists available at ScienceDirect

International Journal of Refrigeration

journal homepage: www.elsevier.com/locate/ijrefrig

Research Paper

Investigation on the regenerative Brayton refrigeration cycle performances using novel Mn-Fe-P-Si composite material with thermal hysteresis as the working medium

Étude des performances du cycle frigorifique régénératif de Brayton utilisant un nouveau matériau composite Mn-Fe-P-Si avec hystérésis thermique comme milieu de travail

Yan Li [a], Bowei Huang [b], Guoxing Lin [a,*], Jincan Chen [a], Ekkes Brück [b]

[a] Department of Physics, Xiamen University, Xiamen 361005, PR China
[b] Fundamental Aspects of Materials and Energy, Department of Radiation Science and Technology, TU Delft, Mekelweg 15, Delft 2629JB, the Netherland

ARTICLE INFO

Keywords:
Mn-Fe-P-Si composite material
Thermal hysteresis
Thermodynamic cycle
Performance evaluation

Mots clés:
Hystérésis thermique
Cycle thermodynamique
Évaluation des performances
Matériau composite Mn-Fe-P-Si

ABSTRACT

MnFeP(As, Ge, Si) series compounds are three kinds of MnFe-based magnetocaloric materials, which have giant magnetocaloric effect. In this work, the experimental characteristic curves of new style Mn-Fe-P-Si materials, numbered as 1: $Mn_{1.32}Fe_{0.67}P_{0.52}Si_{0.49}$, 2: $Mn_{1.37}Fe_{0.63}P_{0.5}Si_{0.5}$, and 3: $Mn_{1.35}Fe_{0.66}P_{0.5}Si_{0.5}$ are presented. Based on the experimental data of these component materials and thermodynamic analysis method, a novel composite material is put forward. The optimal molar mass ratios of the composite material are obtained and they are 0.22, 0.33, 0.45, respectively. A regenerative Brayton refrigeration cycle employing the optimal composite material with thermal hysteresis as the working medium is built. By numerical calculation, the influences of thermal hysteresis on the main thermodynamic quantities are evaluated. The results show that the thermal hysteresis of the working medium results in a decrease of 13.6%, 14.6%, 18.8%, and 16.1% of the cooling quantity, net cooling quantity, optimally working temperature range, and coefficient of performance, respectively. These conclusions are beneficial to the optimal parameter design and performance improvement of active magnetic refrigerators.

1. Introduction

Low-carbon, environmental protection, and the development of new energy have become an important research subject. Solid refrigeration technologies, which use solid materials as refrigerants to achieve refrigeration, have many advantages in saving energy and environment-friendly. Magnetic refrigeration (Arejdal, 2020; He et al., 2020; Lai et al., 2020; Gottschall et al., 2019; Klinar et al., 2019) stands out with its unique advantages among many solid refrigeration technologies. Its refrigeration principle is the magnetocaloric effect (MCE) of magnetic material under magnetic field. The working process of a magnetic refrigerator does not produce any greenhouse gases, which is helpful to slow down the global warming. Therefore, this environment-friendly technology (Greco et al., 2019; Beltrán-López et al., 2019; Franco et al., 2018; Lei et al., 2018; Balli et al., 2017) is worthy to be deeply studied.

In recent years, magnetic refrigeration mainly focused on the studies of room temperature (RT) or near RT magnetic refrigeration theory and technology, including magnetic refrigeration materials and magnetic refrigerators. For RT magnetic refrigerators, Yu et al. (2010) reviewed the magnetic refrigerators built before the year 2010, more than 40 magnetic refrigeration prototypes and their parameters and performances were introduced. Aprea et al. (2017) optimized the energy performances of a magnetic refrigerator by the artificial neural network. Huang et al. (2019) developed a rotary active magnetic regeneration refrigerator prototype for studying the performance of different magnetocaloric materials in a realistic practical environment. Maiorino et al. (2019) analyzed the optimal working performance of magnetic refrigerators. Kamran et al. (2020) used performance evaluation method to estimate the developments of active magnetic regenerative refrigerators. Lu et al. (2019) discussed the heat transfer optimization of

* Corresponding author.
E-mail address: gxlin@xmu.edu.cn (G. Lin).

https://doi.org/10.1016/j.ijrefrig.2021.12.018
Received 9 August 2021; Received in revised form 29 November 2021; Accepted 18 December 2021
Available online 20 December 2021

Nomenclature

B	magnetic field intensity [T]
C_H	specific heat capacity [J K^{-1} kg^{-1}]
Q	quantity of heat [J]
S	magnetic entropy [J K^{-1} kg^{-1}]
T	absolute temperature [K]
W	input work [J]
z	molar mass ratio
1	$Mn_{1.32}Fe_{0.67}P_{0.52}Si_{0.49}$
2	$Mn_{1.37}Fe_{0.63}P_{0.5}Si_{0.5}$
3	$Mn_{1.35}Fe_{0.66}P_{0.5}Si_{0.5}$

Greek letter

Δ	difference
μ_0	Vacuum permeability [F m^{-1}]

Superscript

$'$	low magnetic field
$''$	high magnetic field

Acronyms

Fe	ferrum
Mn	manganese
P	phosphorus
Si	silicon
nre	non-perfect regeneration
rwm	from regenerator to working medium
wmr	from working medium to regenerator

the regenerative magnetic refrigerator by using a topology optimization approach. Li et al. (2021) proposed an active magnetic regenerator with magnetic Brayton cycle in a rotary-magnet type and studied the influence of timing between the magnetic field and the fluid flow. He et al. (2021) developed a three-dimensional micro-unit regeneration magnetic refrigeration model and explored an optimal matching rule of operating parameters. Zhang et al. (2021) reviewed from the perspectives of magnetic refrigeration (MR) thermodynamic cycles and heat transfer enhancement during heat regeneration. With respect to MR cycles, the future trend is likely to be fully solid-state MR cycles and multi-caloric refrigeration cycles. For RT magnetic refrigeration materials, Pecharsky (1997) and Tegus et al. (2002) discovered the giant MCE materials such as $Gd_5Si_2Ge_2$ and $MnFeP_{0.5}As_{0.5}$. Subsequently, more RT or near RT magnetic refrigeration materials were revealed. The MnFe-based compounds with giant MCE were deeply studied (Kavita et al., 2019; Ou et al., 2018; Wurentuya et al., 2018). Brück et al. (2008) described the properties and structure of Mn-based materials used in magnetic refrigeration. Nguyen (2010) researched on MnFeP1-xGex material and discussed the method of reducing thermal hysteresis. Katagiri et al. (2013) explored the magnetocaloric properties and the refrigeration capacity of $MnFeP_{1-x}Si_x$ and obtained the flat entropy-temperature curve of a layered composite material over a wide temperature range of 30 K. Engelbrecht et al. (2013) studied the modeling characteristics and material properties for $MnFeP_{1-x}As_x$ materials. Thang et al. (2017) discussed the performance effects of MnFe(P, Si, B) compounds under different heat treatment conditions. Monfared et al. (2018) indicated the material requirements for the magnetic refrigeration applications called case 1 and case 2 with the limits and assumptions explained in their study. Lai et al. (2018) revealed the microstructure formation and MCE of $(Mn,Fe)_2(P,Si,B)$ alloys. Chen et al. (2020) reported the large magnetic entropy change and refrigeration capacity around RT in quinary $Ni_{41}Co_{9-x}Fe_xMn_{40}Sn_{10}$ alloys (x = 2.0, 2.5). Tu et al. (2022) adopted machine learning methods to predict the magnetocaloric performance of Mn-Fe-P-Si compounds for the first time and their work has the potential to solve the challenges and boost the research of Mn-Fe-P-Si alloys. Perween et al. (2022) investigated the magnetocaloric effect and critical behavior in $Mn_{3-x}Fe_xSn_2$ (x = 0.3, 0.7) alloys synthesized by melting method, further found successive magnetic transitions with large refrigerant capacity in $Mn_{3-x}Fe_xSn_2$ (x = 0.3, 0.7) alloys.

First-order magnetic (FOM) phase transition materials as MnFe-based materials can replace Gd (Tishin et al., 1999), which exhibit giant MCE. However, MnFe-based materials have mostly thermal hysteresis, magnetic hysteresis, and small temperature span with large or giant magnetic entropy change. These factors will affect the performance of magnetic materials in a refrigeration cycle. Thermal hysteresis is an important property of FOM phase transition materials. Its remarkable feature is a separation phenomenon of heating and cooling processes under same magnetic field, and their transition temperatures are also different. The size of thermal hysteresis depends on the difference between the two transition temperatures and it is generally thought as the difference value between the two transition temperatures from the magnetization versus temperature curves under same magnetic field. Thermal hysteresis of working medium material will result in the reduction of magnetic refrigerator performances. Some scholars devoted to exploring the thermal hysteresis in magnetocaloric materials. Skokov et al. (2013) considered the impact of thermal hysteresis on the MCE of $LaFe_{11.6}Si_{1.4}$. Von Moos et al. (2014) established an active magnetic regenerator (AMR) device to study the effect of thermal hysteresis in MnFe(P,As) material. Brown et al. (2016), Hess et al. (2020), and Gutfleisch et al. (2016) studied the influence of thermal hysteresis on the performance of magnetic refrigeration materials. Bessa et al. (2017) described the influence of thermal hysteresis on the performance of a thermomagnetic motor for different materials. Christiaanse et al. (2017) examined six samples of the Mn–Fe–P–Si hysteretic magnetocaloric materials with different transition temperatures. Brown et al. (2018) discussed the effects on the Brayton/Ericsson cycle and hysteresis of magnetic materials. Liu et al. (2019) revealed the origin of low hysteresis in MnNiGe-based system. Christiaanse et al. (2019) compared results obtained from experiments and modeling of single and multi-layer Mn–Fe–Si–P regenerators. Moreover, they proposed a framework, which consider the hysteresis of the material by the numerical model. Govindappa et al. (2021) predicted the thermal hysteresis behavior for a single-layer $MnFeP_{1-x}Si_x$ active magnetic regenerator and compared to experimental data for both a Gadolinium (Gd) and $MnFeP_{1-x}Si_x$ active magnetic regenerator. It is extremely significant to further study the new magnetic refrigeration materials and reveal their thermal hysteresis behavior, especially in some important refrigeration cycles.

Most of MnFe-based magnetocaloric materials have giant MCE and their Curie temperatures are generally near RT. For this reason, they may be considered as the working mediums of RT magnetic refrigerators. However, the peak width at half height of entropy change vs temperature curves of MnFe-based magnetocaloric materials is small and thus single MnFe-based magnetocaloric material is not suitable for the refrigerant of RT magnetic refrigerators. Current researches show that choosing composite material based on several magnetocaloric materials as the working medium of a magnetic refrigerator is an effective method. Especially, for a composite magnetocaloric material, large magnetic entropy change can be ensured and its peak width at half height can be enlarged. This is beneficial to increase greatly refrigeration temperature span of the magnetic refrigerator using composite magnetocaloric material as the working medium.

In this paper, we launch firstly the new Mn-Fe-P-Si magnetocaloric materials named as $Mn_{1.32}Fe_{0.67}P_{0.52}Si_{0.49}$, $Mn_{1.37}Fe_{0.63}P_{0.5}Si_{0.5}$ and

$Mn_{1.35}Fe_{0.66}P_{0.5}Si_{0.5}$. Then, based on the adiabatic temperature change and isothermal magnetic entropy change data from experimental measurements, a novel composite material including portion of $Mn_{1.32}Fe_{0.67}P_{0.52}Si_{0.49}$, $Mn_{1.37}Fe_{0.63}P_{0.5}Si_{0.5}$ and $Mn_{1.35}Fe_{0.66}P_{0.5}Si_{0.5}$ is proposed. Furthermore, new regenerative Brayton refrigeration cycle models are constructed for considering the effect of thermal hysteresis. Finally, the influences of thermal hysteresis on the critical thermodynamic quantities [e.g., cooling quantity, net cooling quantity, and coefficient of performance (*COP*)] are also minutely analyzed.

2. Magnetocaloric properties of the MnFe-based materials with thermal hysteresis

The magnetocaloric characteristics of FOM phase transition magnetocaloric materials are different from those of second-order magnetic phase transition magnetocaloric materials. The specific heat capacities as a function of temperature measured by the DSC method (Jeppesen et al., 2008) for the MnFe-based materials 1, 2 and 3 are displayed in Fig. 1, which shows the heating and cooling processes at constant magnetic fields of 0 T and 1.5 T with black and blue curves, respectively.

Based on the *M*~*H* experimental data of MnFe-based materials, the variations of isothermal magnetic entropy change with temperature can be calculated. For instance, the dependence of the isothermal magnetic entropy changes on the temperature curves are depicted in Fig. 2(a). The adiabatic temperature change and isothermal magnetic entropy change are two critical parameters to characterize the MCE of magnetocaloric materials. Therefore, the direct measurement results of adiabatic temperature changes for the MnFe-based materials are also shown in Fig. 2(b).

3. Optimal design of Mn-Fe-P-Si composite material

The composite material established in this paper is considered to be a kind of physics composite, in which three kinds of component materials are in close contact with each other and their respective chemistries have not been changed. When the composite material as the working medium operates in the Brayton refrigeration cycle, it will experience an adiabatic field change and the temperature of the working medium can attain a stable state, because it is supposed that the direct heat transfer among the component materials can finish in a very short time.

In order to make the best of the MCE of these Mn-Fe-P-Si materials mentioned above, which can be employed as the refrigerants, we should design optimally their molar mass ratios. The composite based on several component MCE materials with the optimal mass ratios will not change the MCE properties of the component materials, but the total entropy change of the composite will learn from others' strong points to offset one's weakness and become flat within certain temperature region. Thus, the non-perfect regeneration in the regenerative Brayton refrigeration cycle using the composite material as the working medium can be greatly decreased. This means that the performance of the regenerative Brayton refrigeration cycle employing the composite material as the working medium will be improved greatly.

Let the optimal molar mass ratios of the composite material as z_1, z_2, and z_3 corresponding to the materials 1, 2, and 3, respectively. The entropy of each Mn-Fe-P-Si material satisfies the additivity principle as an extensive quantity, and the total entropy and total entropy change of

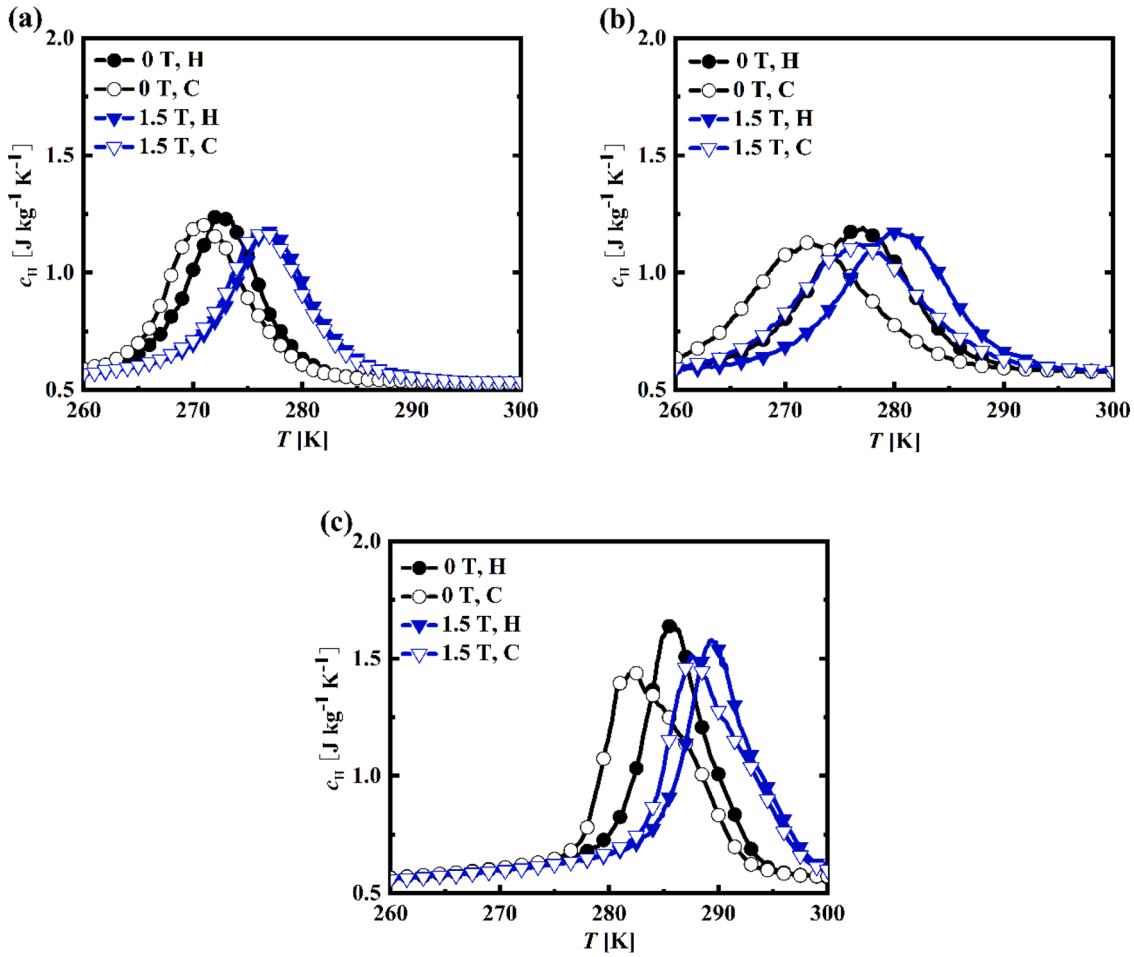

Fig. 1. Specific heat capacity versus temperature curves for (a) $Mn_{1.32}Fe_{0.67}P_{0.52}Si_{0.49}$, (b) $Mn_{1.37}Fe_{0.63}P_{0.5}Si_{0.5}$, and (c) $Mn_{1.35}Fe_{0.66}P_{0.5}Si_{0.5}$ under applied magnetic fields 0 and 1.5 T (H: Heating, C: Cooling) (For interpretation of the references to color in this figure, the reader is referred to the web version of this article.).

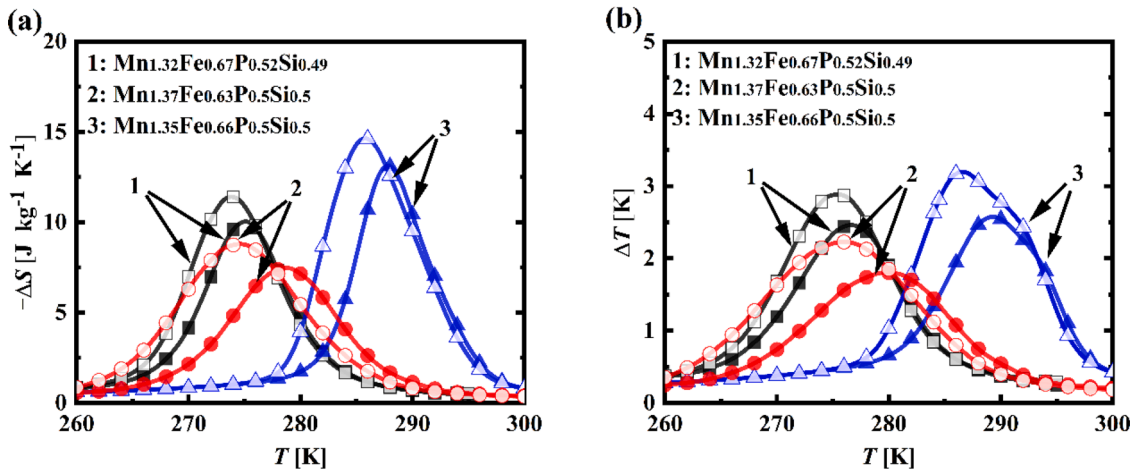

Fig. 2. (a) Isothermal magnetic entropy changes and (b) adiabatic temperature change versus temperature curves for Mn-Fe-P-Si materials with heating (filled symbols) or cooling (open symbols) under 1.5 T field change.

Mn-Fe-P-Si composite material are indicated as:

$$S_{comp} = \sum_{k=1}^{3} z_k S_k(\mu_0 H, T) \tag{1}$$

and

$$\Delta S_{\text{comp}} = \sum_{k=1}^{3} z_k \Delta S_k[\Delta(\mu_0 H), T], \tag{2}$$

where the magnetic field strength is $\mu_0 H$, T is the temperature, the magnetic entropy and magnetic entropy change of the component materials are S and ΔS, respectively.

These Mn-Fe-P-Si component materials are combined into a novel composite material to achieve the goal that the total magnetic entropy changes are close to a "constant", i.e., the mean value of total entropy changes in certain reasonable temperature range. For example, in the reasonable temperature range 275–287 K (flat curve region) shown in Fig. 3, the mean values of total entropy changes of the composite material are 4.8 with thermal hysteresis and 6.0 without thermal hysteresis, and any total entropy change with different temperature in this region is close to this mean value (i.e., so-called constant). For this reason, the molar mass ratios should conform to the following equations (Xu et al., 2015; Smaïli et al. 1997):

$$\begin{aligned}
&\sum_{k=1}^{3} z_k \left[\Delta S_k\left(\Delta\mu_0 H, T_m^{j+1}\right) - \Delta S_k\left(\Delta\mu_0 H, T_m^{j}\right)\right] \\
&= z_1\left[\Delta S_1\left(\Delta\mu_0 H, T_m^{2}\right) - \Delta S_1\left(\Delta\mu_0 H, T_m^{1}\right)\right] + z_2\left[\Delta S_2\left(\Delta\mu_0 H, T_m^{2}\right) - \Delta S_2\left(\Delta\mu_0 H, T_m^{1}\right)\right] + z_3\left[\Delta S_3\left(\Delta\mu_0 H, T_m^{2}\right) - \Delta S_3\left(\Delta\mu_0 H, T_m^{1}\right)\right] \\
&+ z_1\left[\Delta S_1\left(\Delta\mu_0 H, T_m^{3}\right) - \Delta S_1\left(\Delta\mu_0 H, T_m^{2}\right)\right] + z_2\left[\Delta S_2\left(\Delta\mu_0 H, T_m^{3}\right) - \Delta S_2\left(\Delta\mu_0 H, T_m^{2}\right)\right] + z_3\left[\Delta S_3\left(\Delta\mu_0 H, T_m^{3}\right) - \Delta S_3\left(\Delta\mu_0 H, T_m^{2}\right)\right] \\
&= 0 (j = 1, 2)
\end{aligned} \tag{3}$$

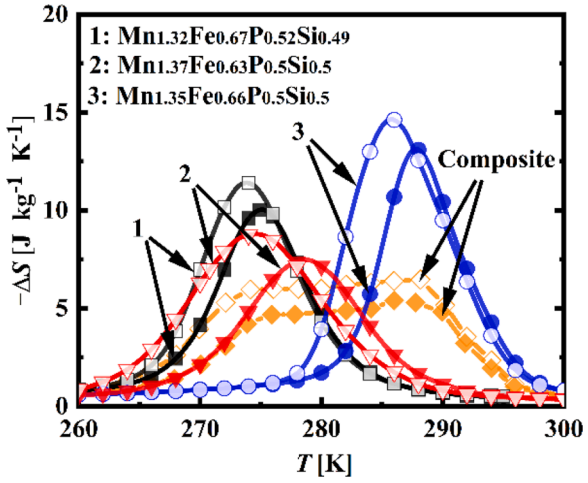

Fig. 3. Isothermal magnetic entropy changes for the Mn-Fe-P-Si composite and component materials varying with temperature under applied magnetic fields 0 and 1.5 T (solid icon: heating; hollow icon: cooling).

and

$$\sum_{k=1}^{3} z_k = 1 \tag{4}$$

where the superscript j represents the types of Mn-Fe-P-Si component materials at different Curie temperatures and its value range is $0 \le j \le$ n-1. According to Eqs. (3) and (4) and the experimental data of Fig. 2, the optimal molar mass ratios of the component magnetocaloric materials can be solved out as follows:

$$z_1 = 0.22, \tag{5}$$

$$z_2 = 0.33, \tag{6}$$

and

$$z_3 = 0.45. \tag{7}$$

If Eqs. (5)–(7) are satisfied, the composite material including the component materials $Mn_{1.32}Fe_{0.67}P_{0.52}Si_{0.49}$, $Mn_{1.37}Fe_{0.63}P_{0.5}Si_{0.5}$ and $Mn_{1.35}Fe_{0.66}P_{0.5}Si_{0.5}$ can maintain a large MCE within a wider temperature range and reduce the effect of non-perfect regeneration in a

regenerative refrigeration cycle.

From Fig. 3, one can find that the composite material has much larger operating temperature region than the component materials whether the thermal hysteresis is considered or not. Although the magnetic entropy of the composite material is decreased, but the *COP* and net cooling quantity in a wide working temperature range will be greatly increased.

4. The regenerative Brayton refrigeration cycle using the composite material as the working medium

4.1. The total entropy curves of the composite material

Combining Eq. (1) and the optimized molar mass ratio with the related experimental data of the component materials, the total entropy S_{comp} vs temperature T characteristic curves (i.e., dot dash and solid lines) for the composite material are obtained by means of numerical calculation, which shows four iso-field entropy-temperature ($S_{comp} \sim T$) curves representing the increasing and decreasing temperature processes under applied magnetic fields 0 and 1.5 T, as shown in Fig. 4. Based on these curves of the total entropy versus temperature, we may establish the different regenerative Brayton refrigeration cycles.

4.2. The regenerative magnetic Brayton refrigeration cycles

Usually, two isomagnetic field and two adiabatic processes constitute a magnetic Brayton refrigeration cycle. In this work, we consider two different regenerative Brayton refrigeration cycles with or without thermal hysteresis, as depicted in Fig. 4(a) and (b). One is constitutive of low-field (0 T) heating ($E_1 \rightarrow A_1$, black solid line), high temperature adiabatic magnetization ($A_1 \rightarrow B_1$), high-field (1.5 T) cooling ($B_1 \rightarrow D_1$, orange solid line), and low temperature adiabatic demagnetization ($D_1 \rightarrow E_1$) processes. These processes constitute the magnetic regenerative Brayton refrigeration cycle without hysteresis ($A_1B_1C_1D_1E_1F_1A_1$) which is shortened as the WOH cycle, as shown in Fig. 4(a). The other consists of low-field (0 T) heating ($E_2 \rightarrow A_2$, black solid line), high temperature adiabatic magnetization ($A_2 \rightarrow B_2$), high-field (1.5 T) cooling ($B_2 \rightarrow D_2$, blue dot dash line), and low temperature adiabatic demagnetization ($D_2 \rightarrow E_2$) processes. These processes constitute the magnetic regenerative Brayton refrigeration cycle with hysteresis ($A_2B_2C_2D_2E_2F_2A_2$) which is shortened as the WH cycle, as shown in Fig. 4(b). In Fig. 4(a) and (b), the heat quantity absorbed from the cold reservoir and heat quantity released to the hot reservoir are Q_{cr} and Q_{hr}, respectively. Q_{wmr} and $Q_{rwm}$are, respectively, the heat quantities released to the regenerator and absorbed from the regenerator. T_m is the temperature corresponding to the maximum magnetic entropy change of the composite material. T_h and T_c are, respectively, the temperatures of hot and cold reservoirs.

From Fig. 4, one can see that there are four iso-field entropy-temperature curves such that four kinds of Brayton refrigeration cycles may be set up between the high and low fields. For the convenience of comparison, based on the entropy-temperature heating curve under 0 T magnetic field, two kinds of regenerative Brayton refrigeration cycles are established in this paper, where the temperatures T_h and T_c of the hot and cold reservoirs are set as 285 K and 275 K . The reason is that (i) the other two kinds of regenerative Brayton refrigeration cycles based on the entropy-temperature cooling curve under 1.5 T magnetic field are similar to the regenerative Brayton refrigeration cycles established in this paper. (ii) It is enough to select two kinds of regenerative Brayton refrigeration cycles for investigating the effects of thermal hysteresis and non-perfect regeneration.

On the basis of the regenerative Brayton refrigeration cycles (WOH or WH cycle) and thermodynamic theory, the heats exchanged in each process can be expressed as follows (Diguet et al., 2012; Li et al., 2021):

$$Q_{cr} = \begin{cases} \int_{T_{E_1}}^{T_{F_1}} C_H(\mu_0 H', T)dT(WOH) \\ \int_{T_{E_2}}^{T_{F_2}} C_H(\mu_0 H', T)dT(WH) \end{cases}, \tag{8}$$

$$Q_{hr} = \begin{cases} -\int_{T_{C_1}}^{T_{B_1}} C_H(\mu_0 H'', T)dT(WOH) \\ -\int_{T_{C_2}}^{T_{B_2}} C_H(\mu_0 H'', T)dT(WH) \end{cases}, \tag{9}$$

$$Q_{wmr} = \begin{cases} \int_{C_1 \rightarrow D_1} TdS = \int_{T_h}^{T_c} C_H(\mu_0 H, T)dT(WOH) \\ \int_{C_2 \rightarrow D_2} TdS = \int_{T_h}^{T_c} C_H(\mu_0 H'', T)dT(WH) \end{cases}, \tag{10}$$

and

$$Q_{rwm} = \begin{cases} \int_{F_1 \rightarrow A_1} TdS = \int_{T_h}^{T_c} C_H(\mu_0 H', T)dT(WOH) \\ \int_{F_2 \rightarrow A_2} TdS = \int_{T_h}^{T_c} C_H(\mu_0 H', T)dT(WH) \end{cases}. \tag{11}$$

For a MnFe-based magnetocaloric material, the non-perfect regenera-

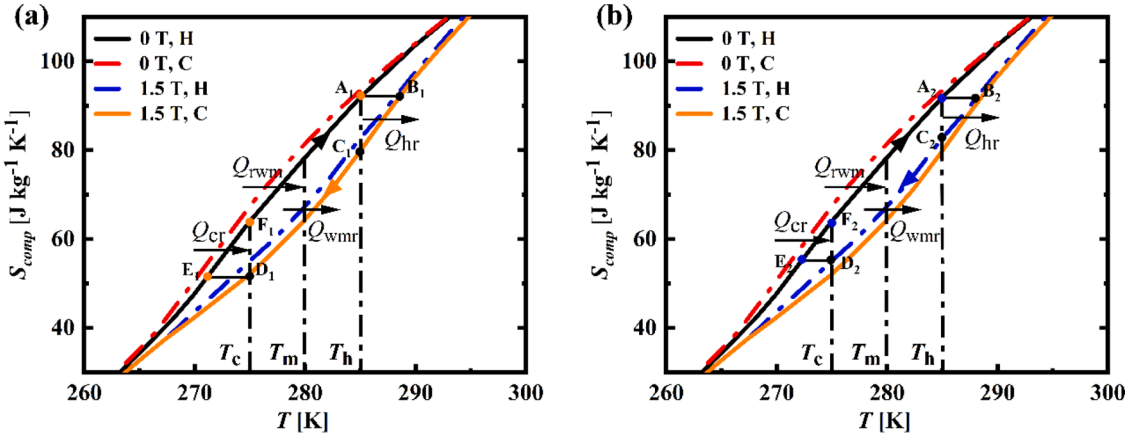

Fig. 4. Total entropy S_{comp} of the composite material varying with temperature T at 0 and 1.5 T magnetic fields and the schematic diagrams of regenerative Brayton refrigeration cycles (a) without or (b) with thermal hysteresis.

tion quantity always exists in the regenerative refrigeration cycle and it has definite effect on the refrigeration cycle performance. It should be pointed out that the non-perfect regeneration quantity in two regenerative processes can be further written as:

$$Q_{\mathrm{nre}} = \int_{T_c}^{T_h} T[dS(\mu_0 H'', T) - dS(\mu_0 H', T)]. \tag{12}$$

Obviously, the non-perfect regeneration quantities coming from the different regenerative Brayton refrigeration cycles are different. We should minimize the influence of the non-perfect regenerative quantity on the WOH or WH cycle performances by related parametric design. In fact, the impact of the non-perfect regenerative quantity on the net cooling quantity can be represented as:

$$Q_{\mathrm{net}} = Q_{cr} - \theta Q_{\mathrm{nre}}, \tag{13}$$

where $\theta = 1$ when $Q_{\mathrm{nre}} \geq 0$ and $\theta = 0$ when $Q_{\mathrm{nre}} < 0$. When $Q_{\mathrm{nre}} < 0$, the impact of the non-perfect regenerative quantity on the net cooling quantity is zero, but its effects on the work input W_B and *COP* cannot be neglected. This can be seen from the following equations:

$$W_B = -(Q_{\mathrm{hr}} + Q_{cr} + Q_{\mathrm{rwm}} + Q_{\mathrm{wmr}}) \tag{14}$$

and

$$COP = \frac{Q_{net}}{W_B}. \tag{15}$$

In next section, the effects of thermal hysteresis on the performance characteristics of the WOH or WH cycle will be discussed in detail.

5. Results and discussion

According to the above discussion, the influences of thermal hysteresis on the main thermodynamic quantities (e.g. cooling quantity, net cooling quantity and *COP*) in the regenerative Brayton refrigeration cycle employing the composite material as the working medium will be emphatically evaluated.

5.1. Cooling quantity Q_{cr}

By using Eq. (8) and Fig. 1, the Q_{cr} versus T_{c} curves for the different regenerative Brayton refrigeration cycles employing the composite material as the working medium are obtained, as displayed in Fig. 5. It is observed from Fig. 5 that T_m' of composite material with thermal hysteresis is 280.0 K and T_m of the composite material without thermal hysteresis is 282.0 K. The maximum cooling quantities with and without thermal hysteresis are 1459 J kg^{-1} and 1689 J kg^{-1}, respectively. It follows that the thermal hysteresis directly results in decreasing the maximum cooling quantity by 13.6%. The thermal hysteresis will also lead to the decrease of the suitable operating temperature span in the regenerative Brayton refrigeration cycle. For example, the suitable operating temperature range of the WOH cycle is 16 K, while that of the WH cycle is 13 K. Therefore, the thermal hysteresis leads to reducing the optimal operating temperature range by 18.8% in the regenerative Brayton refrigeration cycle.

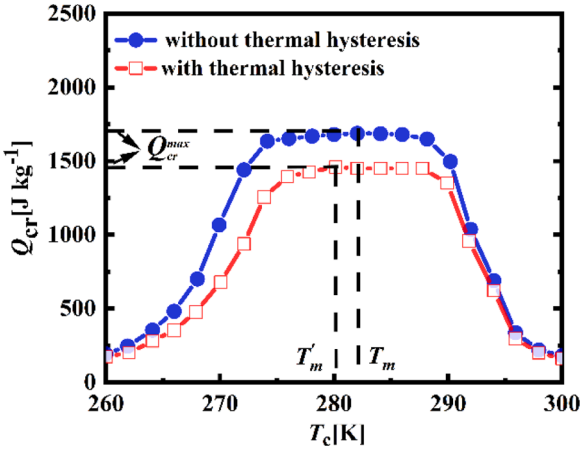

Fig. 5. The curves of Q_{cr} varying with T_{c} in the regenerative Brayton refrigeration cycles employing the composite material as the working medium without or with thermal hysteresis.

5.2. Net cooling quantity Q_{net}

In a regenerative Brayton refrigeration cycle, the net cooling quantity Q_{net} is always not greater than the cooling quantity Q_{cr}. Fig. 6(a)–(d) indicate the curves of the cooling quantity Q_{cr} and net cooling quantity Q_{net} varying with T_{c} for different hot reservoir temperatures. In Fig. 6(a), when $T_h = T_m - 2K$or $T_h = T_m' - 2K$, the non-perfect regeneration does not affect net cooling quantity, but affects the *COP*. Under the above conditions, the cooling quantity is always equal to the net cooling quantity regardless of whether thermal hysteresis is considered or not in the regenerative Brayton refrigeration cycles (WOH or WH cycle).

When $T_h = T_{\mathrm{m}}(T_m') + 2K, T_{\mathrm{m}}(T_m') + 4$Kor $T_{\mathrm{m}}(T_m') + 6$K, the net cooling quantities varies with the change of non-perfect regenerative quantity, as indicated in Fig. 6(b)–(d). In these cases, the net cooling quantity is always not greater than the cooling quantity. Furthermore, when$T_{\mathrm{c}} < T_m(T_m') < T_{\mathrm{h}}$, with the increase of T_{c}, the net cooling quantity also rapidly increases. When the T_{c} reaches T_{m} (or T_m'), the net cooling quantity tends to be relatively flat. While$T_{\mathrm{m}}(T_m') < T_{\mathrm{c}} < T_{\mathrm{h}}$, the net cooling quantity is greatly affected by the non-perfect regenerative quantity in the regenerative Brayton refrigeration cycle. As depicted in Fig. 6(b)–(d), the difference of the net cooling quantities of the cycles without or with thermal hysteresis increases with the increase of T_{c} and then tends to stable constant when it reaches $T_{\mathrm{h}} > T_{\mathrm{c}} > T_{\mathrm{m}}(T_m')$, e.g., the difference of the net cooling quantities is 336.0 J kg^{-1} at T_{c}=280.0 K and 399.0 J kg^{-1} at T_{c}=285.0 K.

On the other hand, with the increase of the hot reservoir temperature T_{h}, the net cooling quantity in the WOH or WH cycle significantly decreases for a fixed cold reservoir temperature T_{c}, because the cooling quantity is related directly to the cold reservoir temperature T_{c} and the non-perfect regenerative quantity generally corresponds to the net cooling quantity. With the increase of T_{h}, the non-perfect regenerative quantity of the WOH or WH cycle increases.

The numerical calculation results of the main thermodynamic quantities for the WOH or WH cycle employing the component or composite material as the working medium are listed in Tables 1, 2, 3, 4. It can be seen from Tables 1–4 that, at the same operating condition, the net cooling quantity Q_{net} and *COP* of the WH cycle are always smaller than those of the WOH cycle. Q_{net} and *COP* of the WOH or WH cycle operating in $T_{\mathrm{m}}(T_m') \sim T_{\mathrm{m}}(T_m')+4$ K, which are the right side of T_{m} (or T_m'), are always largest. As an example, when the WOH or WH cycle employing the composite as the working medium without thermal hysteresis is set up on the right side of T_{m}, the net cooling quantity can reach 1561 J kg^{-1}. Similarly, the net cooling quantity with thermal hysteresis is 1333 J kg^{-1}. The thermal hysteresis results in decreasing Q_{net} of the composite material by 14.6%. Meanwhile, the thermal hysteresis lead to the decrease of Q_{net} of the component materials 1, 2 and 3 by 3.5%, 20.4%, and 12.4%, respectively. Therefore, the optimal parameter design for a WOH or WH cycle is extremely significant for improving main thermodynamic quantities.

5.3. Coefficient of performance

Fig. 7 shows the curves of the *COP* versus T_{c} for the WOH or WH cycle employing the composite or component materials as the working

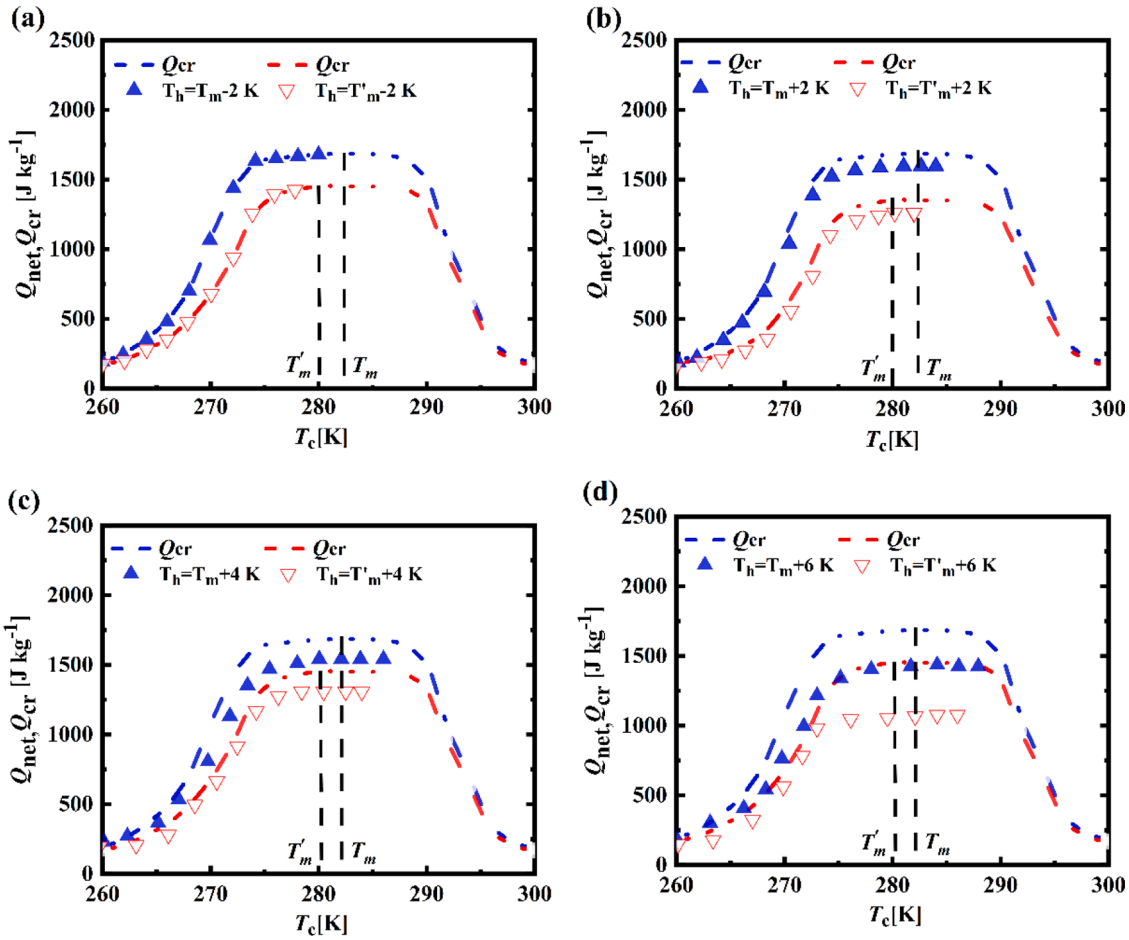

Fig. 6. The Q_{net} and Q_{cr} varying with T_c curves of the WOH or WH cycle employing the composite material as the working medium for a fixed T_h with (red) or without (blue) thermal hysteresis (For interpretation of the references to color in this figure legend, the reader is referred to the web version of this article.).

Table 1
The main thermodynamic quantities in the WOH or WH cycle employing the composite material as the working medium, where $\Delta H = 0\sim1.5$ T.

with thermal hysteresis				without thermal hysteresis		
T_c	T'_m-4 K	T'_m-2 K	T'_m	T_m-4 K	T_m-2 K	T_m
T_h	T'_m	T'_m+2 K	T'_m+4 K	T_m	T_m+2 K	T_m+4 K
Q_{cr} (J kg^{-1})	1295	1326	1459	1558	1589	1689
-Q_{hr} (J kg^{-1})	1459	1452	1449	1689	1684	1681
Q_{nre} (J kg^{-1})	-775.0	-742.0	126.5	-860.0	-814.5	125.0
Q_{net} (J kg^{-1})	1295	1209	1333	1558	1450	1561
W_B (J kg^{-1})	975.0	868.0	116.5	991.0	909.5	120.0
COP	1.33	1.39	11.44	1.57	1.59	13.01

Table 2
The main thermodynamic quantities in the WOH or WH cycle employing $Mn_{1.32}Fe_{0.67}P_{0.52}Si_{0.49}$ as the working medium, where $\Delta H = 0\sim1.5$ T.

with thermal hysteresis				without thermal hysteresis		
T_c	T'_m-4 K	T'_m-2 K	T'_m	T_m-4 K	T_m-2 K	T_m
T_h	T'_m	T'_m+2 K	T'_m+4 K	T_m	T_m+2 K	T_m+4 K
Q_{cr} (J kg^{-1})	1195	1227	1672	1260	1305	1710
-Q_{hr} (J kg^{-1})	1672	1646	1639	1710	1698	1690
Q_{nre} (J kg^{-1})	-890.0	-905.0	447.0	-962.0	-937.0	440.0
Q_{net} (J kg^{-1})	1195	1100	1225	1260	1196	1270
W_B (J kg^{-1})	1367	1324	414.0	1412	1330	420.0
COP	0.87	0.83	2.96	0.89	0.90	3.02

medium. When the cold reservoir temperature T_c gradually increases, the *COP* in the WOH or WH cycle monotonously increases. When T_c=270.0 K and $T_h = T_m(T'_m) - 2K$, the *COP* of the WOH cycle with the composite material is 11.8, while that of the WH cycle is 9.9. The thermal hysteresis results in decreasing the *COP* of the composite material by 16.1%. At the same time, when the cold reservoir temperature T_c is 275.0 K or 280.0 K, no matter whether the thermal hysteresis in the Brayton refrigeration cycles is considered or not, the same trend will get for different temperature T_h. For convenient comparison, the *COP*s of the cycle with component materials in Fig. 7 only involve the case for $T_h = T_m(T'_m) + 4K$. When T_c=275.0 K and $T_h = T_m(T'_m) + 4K$, the *COP*s of the WOH cycle with composite or the component materials 1, 2 and 3 are 7.65, 4.32, 3.10 and 2.20, respectively; while those in the WH cycle are 6.15, 3.85, 2.62, and 1.60. The thermal hysteresis results in decreasing the *COP* of the cycle with composite material by 19.6%. The thermal hysteresis results in decreasing the *COP*s of the cycle with the component materials 1, 2 and 3 by 10.9%, 15.5%, and 27.3%, respectively. Regardless of whether thermal hysteresis is considered or not, it is obvious that the *COP* of the refrigeration cycle with the composite material is always larger than those with the component materials.

For a near RT magnetic refrigeration prototype (Ames Laboratory in US), its *COP* can achieve 75% of the COP_{Carnot} (Gschneidner Jr et al. 2005). It has been reported that the *COP* of the proof-of-principle magnetic refrigerator in Ames Laboratory achieved a cooling power of 600 W with a *COP* approaching 15 (Gschneidner Jr et al. 2006). The value of the *COP* in Table 1 is still somewhat large. This value arises in

Table 3
The main thermodynamic quantities in the WOH or WH cycle employing $Mn_{1.37}Fe_{0.63}P_{0.5}Si_{0.5}$ as the working medium, where $\Delta H = 0{\sim}1.5$ T.

with thermal hysteresis				without thermal hysteresis		
T_c	T'_m-4 K	T'_m-2 K	T'_m	T_m-4 K	T_m-2 K	T_m
T_h	T'_m	$T'_m + 2$ K	$T'_m + 4$ K	T_m	T_m+2 K	T_m+4 K
Q_{cr} (J kg^{-1})	1202	1240	1722	1525	1691	2035
-Q_{hr} (J kg^{-1})	1722	1704	1659	2035	1991	2016
Q_{nre} (J kg^{-1})	-821.0	-805.0	436.0	-836.0	-809.8	419.0
Q_{net} (J kg^{-1})	1202	1103	1286	1525	1167	1616
W_B (J kg^{-1})	1341	1269	373.0	1346	1311	400.0
COP	0.90	0.87	3.45	1.13	0.89	3.94

Table 4
The main thermodynamic quantities in the WOH or WH cycle employing $Mn_{1.35}Fe_{0.66}P_{0.5}Si_{0.5}$ as the working medium, where $\Delta H = 0{\sim}1.5$ T.

with thermal hysteresis				without thermal hysteresis		
T_c	T'_m-4 K	T'_m-2 K	T'_m	T_m-4 K	T_m-2 K	T_m
T_h	T'_m	$T'_m + 2$ K	$T'_m + 4$ K	T_m	T_m+2 K	T_m+4 K
Q_{cr} (J kg^{-1})	412.0	507.0	1382	528.0	572.4	1503
-Q_{hr} (J kg^{-1})	1382	1360	1327	1503	1409	1470
Q_{nre} (J kg^{-1})	-545.0	-511.0	402.5	-581.0	-556.0	385
Q_{net} (J kg^{-1})	412.0	313.0	979.5	528.0	442.5	1118
W_B (J kg^{-1})	1515	1364	347.5	1556	1393	352.0
COP	0.27	0.23	2.82	0.34	0.32	3.18

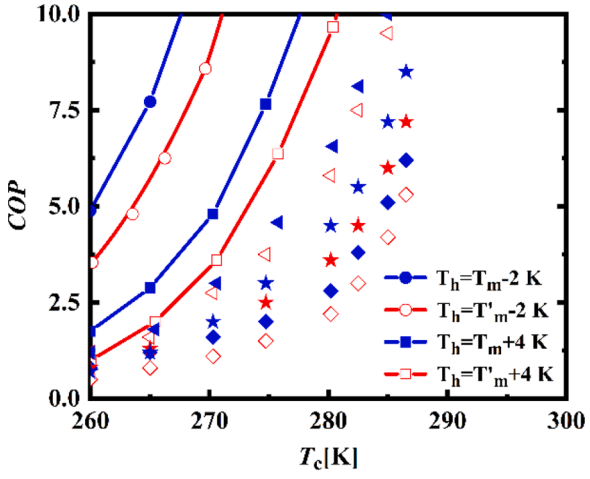

Fig. 7. The *COP* versus T_c curves in the WOH or WH cycle (WOH: blue; WH: red) employing the composite (circle and square) or component materials (1: $Mn_{1.32}Fe_{0.67}P_{0.52}Si_{0.49}$: rhombus; 2: $Mn_{1.37}Fe_{0.63}P_{0.5}Si_{0.5}$: triangle; and 3: $Mn_{1.35}Fe_{0.66}P_{0.5}Si_{0.5}$: star) as the working medium for given T_h (For interpretation of the references to color in this figure legend, the reader is referred to the web version of this article.).

the regenerative Brayton refrigeration cycles using the composite material as the working medium. This is because the regenerative Brayton refrigeration cycles with the composite material are close to perfect regeneration such that the *COP* is close to COP_{Carnot}. Of course, if the other irreversibility in actual magnetic refrigeration systems are further considered, the *COP* will distinctly decrease.

6. Conclusions

In the present paper, a novel composite material including $Mn_{1.32}Fe_{0.67}P_{0.52}Si_{0.49}$, $Mn_{1.37}Fe_{0.63}P_{0.5}Si_{0.5}$ and $Mn_{1.35}Fe_{0.66}P_{0.5}Si_{0.5}$ is optimally designed, and its working temperature range is significantly improved. The curves of the total entropy S_{comp} varying with temperature T for the composite material under applied magnetic fields 0 and 1.5 T are determined, and the WOH or WH cycle model is established. Furthermore, the thermodynamic performances influenced by thermal hysteresis in the WH cycle employing the composite material as the working medium are evaluated. The research results show that the thermal hysteresis lead to the decrease 13.6% of the cooling quantity, 14.6% of the net cooling quantity Q_{net}, and 18.8% of the optimal working temperature range, respectively. With the increase of hot reservoir temperature T_h, the net cooling quantity in the WOH or WH cycle significantly decreases for a determined cold reservoir temperature T_c. When T_c=270.0 K and $T_h = T_m(T'_m) - 2K$, Thermal hysteresis will also reduce the *COP* in the regenerative Brayton refrigeration cycle, which results in the decrease 16.1% of the *COP*. When T_c=275.0 K and $T_h = T_m(T'_m) + 4K$, the thermal hysteresis leads to a 19.6% reduction in the *COP* of the composite material. These research results will provide powerful support for the Mn-Fe-P-Si composite material as a promising working medium in RT magnetic refrigeration applications.

It should be pointed out that, in the present paper, we only take the regenerative Brayton refrigeration cycle performance with thermal hysteresis into account, and have not discussed the impacts of the internal irreversibility of the working medium and heat-transfer irreversibility between the working medium and the heat reservoirs, the heat conductivity, the different parts of heat capacity and the shape of AMR material, etc. on the performance of RT magnetic refrigeration systems, which will be further work to be considered in actual RT magnetic refrigeration systems. These factors will have different degrees of influences on the main thermodynamic performances of refrigeration cycles. For example, if heat-transfer irreversibility between the working medium and the high/low temperature heat reservoir are considered, the net cooling quantity and *COP* of the regenerative Brayton refrigeration cycle will decrease greatly. For this reason, heat-exchange fluid with the heat conductivity as possible as large should be selected in order to improve refrigeration performance. If the shape of solid refrigerant or regenerative material is not machined as spherical granules with millimeter diameter, its corresponding refrigeration performance will also get worse. Moreover, the heat capacity of heat-transfer fluid in a magnetic refrigeration system should be larger than that of the working medium or regenerative material.

Declaration of Competing Interest

The authors declare that they have no known competing financial interests or personal relationships that could have appeared to influence the work reported in this paper.

Acknowledgments

This work has been supported by the National Natural Science Foundation (Grant No. 51776178), People's Republic of China. And the authors would like to thank for the data provided by BASF.

References

Aprea, C., Greco, A., Maiorino, A., 2017. An application of the artificial neural network to optimise the energy performances of a magnetic refrigerator. Int. J. Refrig. 82, 238–251.
Arejdal, M., 2020. Prediction of the magnetocaloric behaviors of the Kekulene structure for the magnetic refrigeration. Results Phys. 18, 103342.
Beltrán-López, J.F., Palacios, E., Velázquez, D., Burriel, R., 2019. Design and optimization of a magnet for magnetocaloric refrigeration. J. Appl. Phys. 126 (16), 164502.

Brown, T.D., Buffington, T., Shamberger, P.J., 2018. Effects of hysteresis and Brayton cycle constraints on magnetocaloric refrigerant performance. J. Appl. Phys. 123 (18), 185101.
Balli, M., Jandl, S., Fournier, P., Kedous-Lebouc, A., 2017. Advanced materials for magnetic cooling: fundamentals and practical aspects. Appl. Phys. Rev. 4 (2), 021305.
Bessa, C.V.X., Ferreira, L.D.R., Horikawa, O., Monteiro, J.C.B., Gandra, F.G., Gama, S., 2017. On the influence of thermal hysteresis on the performance of thermomagnetic motors. J. Appl. Phys. 122 (24), 244502.
Brown, T.D., Karaman, I., Shamberger, P.J., 2016. Impact of cycle-hysteresis interactions on the performance of giant magnetocaloric effect refrigerants. Mater. Res. Express. 3 (7), 074001.
Brück, E., Tegus, O., Cam Thanh, D.T., Trung, N.T., Buschow, K.H.J., 2008. A review on Mn based materials for magnetic refrigeration: structure and properties. Int. J. Refrig. 31 (5), 763–770.
Chen, F., Sánchez Llamazares, J.L., Sánchez-Valdés, C.F., Chen, F.H., Li, Z.B., Tong, Y.X., Li, L., 2020. Large magnetic entropy change and refrigeration capacity around room temperature in quinary $Ni_{41}Co_{9-x}Fe_xMn_{40}Sn_{10}$ alloys (x= 2.0 and 2.5). J. Alloy. Compd. 825, 154053.
Christiaanse, T.V., Trevizoli, P.V., Rowe, A., 2019. Modelling two layer Mn-Fe-Si-P materials in an active magnetic regenerator. Int. J. Refrig. 106, 225–235.
Christiaanse, T.V., Campbell, O., Trevizoli, P.V., Misra, S., van Asten, D., Zhang, L., Govindappa, P., Niknia, I., Teyber, R., Rowe, A., 2017. A concise approach for building the s-T diagram for Mn-Fe-P-Si hysteretic magnetocaloric material. J. Phys. D. Appl. Phys. 50, 365001.
Diguet, G., Lin, G.X., Chen, J.C., 2012. Performance characteristics of magnetic Brayton refrigeration cycles using Gd, Gd0.74Tb0.26 and (Gd3.5Tb1.5) Si4 as the working substance. Int. J. Refrig. 35, 1035–1042.
Engelbrecht, K., Nielsen, K.K., Bahl, C.R.H., Carroll, C.P., van Asten, D., 2013. Material properties and modeling characteristics for MnFeP1−xAsx materials for application in magnetic refrigeration. J. Appl. Phys. 113 (17), 173510.
Franco, V., Blázquez, J.S., Ipus, J.J., Law, J.Y., Moreno-Ramírez, L.M., Conde, A., 2018. Magnetocaloric effect: from materials research to refrigeration devices. Prog. Mater. Sci. 93, 112–232.
Govindappa, P., Trevizoli, P.V., Niknia, I., Christiaanse, T.V., Teyber, R., Rowe, A., 2021. Predicting the thermal hysteresis behavior for a single-layer MnFeP1-xSix active magnetic regenerator. Appl. Therm. Eng. 183, 116173.
Gottschall, T., Skokov, K.P., Fries, M., Taubel, A., Radulov, I., Scheibel, F., Benke, D., Riegg, S., Gutfleisch, O., 2019. Making a cool choice: the materials library of magnetic refrigeration. Adv. Energy Mater. 34 (9), 1901322.
Greco, A., Aprea, C., Maiorino, A., Masselli, C., 2019. A review of the state of the art of solid-state caloric cooling processes at room-temperature before 2019. Int. J. Refrig. 106, 66–88.
Gutfleisch, O., Gottschall, T., Fries, M., Benke, D., Radulov, I., Skokov, K.P., Wende, H., Gruner, M., Acet, M., Entel, P., Farle, M., 2016. Mastering hysteresis in magnetocaloric materials. Philos. Trans. R. Soc. A 374 (2074), 20150308. Math. Philos. T. R. Soc. A.
Gschneidner Jr, K.A., Pecharsky, V.K., 2006. Rare Earths and magnetic refrigeration. J. Rare Earths 24 (6), 641–647.
Gschneidner Jr, K.A., Pecharsky, V.K., Tsokol, A.O., 2005. Recent developments in magnetocaloric materials. Rep. Prog. Phys. 68 (6), 1479–1539.
He, J., Wu, J., Zhang, H., Zhang, Y., Lu, B., 2021. Numerical simulation of a fully solid-state micro-unit regeneration magnetic refrigerator with micro Peltier elements. Appl. Therm. Eng. 186, 116545.
He, J., Wu, J.H., Lu, B.W., Liu, C.P., 2020. Comparative study on the series, parallel, and cascade cycles of a multi-mode room temperature magnetic refrigeration system. Int. J. Refrig. 117, 94–103.
Hess, T., Maier, L.M., Bachmann, N., Corhan, P., Schäfer-Welsen, O., Wöllenstein, J., Bartholomé, K., 2020. Thermal hysteresis and its impact on the efficiency of first-order caloric materials. J. Appl. Phys. 127 (7), 075103.
Huang, B., Lai, J.W., Zeng, D.C., Zheng, Z.G., Harrison, B., Oort, A., van Dijk, N.H., Brück, E., 2019. Development of an experimental rotary magnetic refrigerator prototype. Int. J. Refrig. 104, 42–50.
Jeppesen, S., Linderoth, S., Pryds, N., Theil Kuhn, L., Buch Jensen, J., 2008. Indirect measurement of the magnetocaloric effect using a novel differential scanning calorimeter with magnetic field. Rev. Sci. Instrum. 79 (8), 08390.
Klinar, K., Tomc, U., Jelenc, B., Nosan, S., Kitanovski, A., 2019. New frontiers in magnetic refrigeration with high oscillation energy-efficient electromagnets. Appl. Energy 236, 1062–1077.
Kamran, M.S., Ahmad, H.O., Wang, H.S., 2020. Review on the developments of active magnetic regenerator refrigerators evaluated by performance. Renew. Sustain. Energy Rev. 133, 110247.
Kavita, S., Anusha, G., Bhatt, P., Suresh, V., Vijay, R., Sethupathi, K., Gopalan, R., 2019. On the giant magnetocaloric and mechanical properties of Mn–Fe–P–Si−Ge alloy. J. Alloy. Compd. 153232.
Katagiri, K., Nakamura, K., Wada, H., 2013. Magnetocaloric properties and magnetic refrigerant capacity of MnFeP1−xSix. J. Alloy. Compd. 553, 286–290.
Lai, J.W., Tang, X., Sepehri-Amin, H., Hono, K., 2020. Tuning transition temperature of magnetocaloric Mn1.8Fe0.2(P0.59Si0.41) alloys for cryogenic magnetic refrigeration. Scr. Mater 183, 127–132.
Lei, T., Navickaitė, K., Engelbrecht, K., Barcza, A., Vieyra, H., Nielsen, K.K., Bahl, C.R.H., 2018. Passive characterization and active testing of epoxy bonded regenerators for room temperature magnetic refrigeration. Appl. Therm. Eng. 128, 10–19.
Lu, B.W., Wu, J.H., He, J., Huang, J.H., 2019. Heat transfer optimization of a fully solid state microunit regeneration magnetic refrigerator. Int. J. Refrig. 98, 42–50.
Lai, J.W., Zheng, Z.G., Huang, B.W., Yu, H.Y., Qiu, Z.G., Mao, Y.L., Zhang, S., Xiao, F.M., Zeng, D.C., Goubitz, K., Brück, E., 2018. Microstructure formation and magnetocaloric effect of the Fe2P-type phase in (Mn, Fe)2(P, Si, B) alloys. J. Alloy. Compd. 735, 2567–2573.
Liu, J., Gong, Y.Y., You, Y.R., You, X.M., Huang, B.W., Miao, X.F., Xu, G.Z., Xu, F., Brück, E., 2019. Giant reversible magnetocaloric effect in MnNiGe-based materials: minimizing thermal hysteresis via crystallographic compatibility modulation. Acta Mater. 174, 450–458.
Li, Y., Lin, G.X., Chen, J.C., 2021a. Numerical investigation and performance evaluation of the MnFe-based composite magnetocaloric material with large magnetic entropy change over a wide temperature range. Int. J. Refrig. 121, 61–71.
Li, Z., Li, K., Guo, X., Gao, X., Dai, W., Gong, M., Shen, J., 2021b. Influence of timing between magnetic field and fluid flow in a rotary magnetic refrigerator. Appl. Therm. Eng. 187, 116477.
Maiorino, A., Mauro, A., Del Duca, M.G., Mota-Babiloni, A., Aprea, C., 2019. Looking for energy losses of a rotary permanent magnet magnetic refrigerator to optimize its performances. Energies 12 (22), 4388.
Monfared, B., Palm, B., 2018. Material requirements for magnetic refrigeration applications. Int. J. Refrig. 96, 25–37.
Nguyen, T.T., 2010. First-order Phase Transitions and Giant Magnetocaloric Effect. Delft University of Technology, Delft, pp. 36–57.
Ou, Z.Q., Dung, N.H., Zhang, L., Caron, L., Torun, E., van Dijk, N.H., Tegus, O., Brück, E., 2018. Transition metal substitution in Fe_2P-based $MnFe_{0.95}P0.50Si_{0.50}$ magnetocaloric compounds. J. Alloy. Compd. 730, 392–398.
Pecharsky, V.K., Gschneidner Jr, K.A., 1997. Giant magnetocaloric effect in Gd5 (Si2Ge2). Phys. Rev. Lett. 78, 4494–4497.
Perween, S., Lalita, Rathi, A., Pant, R. P., Gahtori, B., Babu, P.D., Basheed, G.A., 2022. Successive magnetic transitions with large refrigerant capacity in arc-melted Mn3−xFexSn2 (x=0.3, 0.7) alloys. J. Magn. Magn. Mater. 541, 168466.
Skokov, K.P., Müller, K.-H., Moore, J.D., Liu, J., Karpenkov, A.Yu., Krautz, M., Gutfleisch, O., 2013. Influence of thermal hysteresis and field cycling on the magnetocaloric effect in LaFe11.6Si1.4. J. Alloy. Compd. 552, 310–317.
Smaïli, A., Chahine, R., 1997. Composite materials for Ericsson-like magnetic refrigeration cycle. J. Appl. Phys. 81 (2), 824–829.
Tu, D., Yan, J., Xie, Y., Li, J., Feng, S., Xia, M., Li, J., Leung, A.P., 2022. Accelerated design for magnetocaloric performance in Mn-Fe-P-Si compounds using machine learning. J. Mater. Sci. Technol. 96, 241–247.
Tegus, O., Brück, E., Buschow, K.H.J., de Boer, F.R., 2002. Transition-metal-based magnetic refrigerants for room-temperature applications. Nature 415, 150–152.
Thang, N.V., Yibole, H., van Dijk, N.H., Brück, E., 2017. Effect of heat treatment conditions on MnFe (P, Si, B) compounds for room-temperature magnetic refrigeration. J. Alloy. Compd. 699, 633–637.
Tishin, A.M., Gschneidner Jr, K.A., Pecharsky, V.K., 1999. Magnetocaloric effect and heat capacity in the phase-transition region. Phys. Rev. B 59 (1), 503.
Von Moos, L., Nielsen, K.K., Engelbrecht, K., Bahl, C.R.H., 2014. Experimental investigation of the effect of thermal hysteresis in first order material MnFe(P,As) applied in an AMR device. Int. J. Refrig. 37, 303–306.
Wurentuya, B., Yibole, H., Guillou, F., Ou, Z., Zhang, Z., Tegus, O., 2018. First-order magnetic transition, magnetocaloric effect and moment formation in MnFe(P,Ge) magnetocaloric materials revisited by x-ray magnetic circular dichroism. Physica B 544, 66–72.
Xu, Z.C., Lin, G.X., Chen, J.C., 2015. A GdxHo1−x−based composite and its performance characteristics in a regenerative Ericsson refrigeration cycle. J. Alloy Compd. 639, 520–525.
Yu, B., Liu, M., Egolf, P.W., Kitanovski, A., 2010. A review of magnetic refrigerator and heat pump prototypes built before the year 2010. Int. J. Refrig. 33 (6), 1029–1060.
Zhang, Y., Wu, J., He, J., Wang, K., Yu, G., 2021. Solutions to obstacles in the commercialization of room-temperature magnetic refrigeration. Renew. Sustain. Energy Rev. 143, 110933.